Journal of Hydroscience and Hydraulic Engineering
Vol. 3, No. 2, November, 1985, pp.31-47.

CHARACTERISTICS OF CONCURRENCE OF RAINFALL, FLOOD AND STORM SURGE ASSOCIATED WITH TYPHOON

By

Michio Hashino

Professor, Department of Construction Engineering
The University of Tokushima, Tokushima 770, Japan

and

Tohru Kanda

Associate Professor, Department of Civil Engineering
Kobe University, Kobe 657, Japan

SYNOPSIS

The characteristics of concurrence of rainfall and storm surge at Osaka are made clear by analyzing the available data of typhoons for the period 1900-1980. Distributions of typhoon locations when the maximum storm surge η_{max} or the peak rainfall intensity r_p occurred, a histogram of time-lag between η_{max} and r_p, and relationships between η_{max} and r_p, and between η_{max} and the total rainfall R_T are shown. Predictors against the rainfall and the storm surge are selected by using a stepwise regression analysis, and the probability distributions of the residuals are examined. It is estimated with a reasonable possibility that the flood wave due to a heavy rainfall travels down a river and the storm surge invades the river with a short time-lag. The concurrent effect of flood flow and storm surge is quantitatively evaluated, and the characteristics of high water level distribution along the river are examined in terms of the behavior of storm surges running up the tidal reach.

INTRODUCTION

The urban river system in a low-lying land generally consists of the complicated channel networks whose lower reaches are influenced by tides and the invasion of surges whenever storms take place. In such a tidal river, it is probable that a flood flow travels down and a storm surge runs up the river with a considerably short time-lag when a typhoon attacks its basin. In designing the levees of river channels, however, special consideration has been hardly given to the concurrence of flood flow and storm surge, so far. Therefore, the rivers in a highly urbanized area are in serious danger of the extensive damage of inundation caused by both floods and storm surges, in the light of experience of the past typhoon disasters, for example, the Isewan Typhoon. To protect the river basins from such damages, the characteristics of concurrence of rainfall, flood and storm surge associated with a typhoon should be clarified and be effectively applied to planning and management of the flood control system.

In this paper, the characteristics of concurrence of rainfall and storm surge at Osaka are shown as a result of analyzing the available data of typhoons for the period 1900-1980. Predictors against the rainfall and the storm surge are selected by using a stepwise regression analysis on the basis of typhoon track, velocity, central pressure, etc. The concurrent effect of flood flow and storm surge is quantitatively evaluated, and the mechanism of interaction between them in a river is revealed through close analyses of the running-up behavior of storm surges.

CHARACTERISTICS OF CONCURRENCE OF RAINFALL AND STORM SURGE AT OSAKA

Data Utilized for the Analysis

About 460 typhoon cases during the period 1900-1980 were collected for the rectangular area, latitudes 28-40°N and longitudes 128-140°E. For each typhoon, not only the track map and hourly typhoon information (location, central pressure, moving direction and moving velocity), but also the observed data of the hourly tides at Osaka Port and the hourly rainfall, pressure, wind direction and wind velocity at Osaka Meteorological Observatory were collected. The storm surges were determined by subtracting the hourly astronomical tides from the hourly observed tides. As for the rainfall associated with a typhoon, collection of data is confined to the rainfall caused mainly by the typhoon storm structure itself. Thus, the so-called antecedent rainfall, which occurs 7 hours or more prior to the typhoon rainfall, is excluded from the data collection, because the corresponding typhoon under consideration locates far way from Osaka district.

The frequencies of the maximum storm surge η_{max} and the total rainfall R_T are shown in Table 1 regarding the specified values: η_{max}=26 cm and R_T=20 mm. The number of typhoons, that brought storm surges with the peak over 26 cm at Osaka Port, is 35 for the period 1900-1949 and 82 for the period 1950-1980. For the latter period almost all typhoons with the maximum storm surges over 26 cm are picked up, while for the former period a considerable number of storm surge data seem to be unfortunately missed, because the tidal observations are unavailable, or because data of storm surges except those which brought disasters are hardly found out. The courses of typhoons are divided into two groups: east course and west course of the apse line of Osaka Bay as indicated by the dotted line in Fig. 2. In Table 2 which indicates the frequency of η_{max} for each typhoon course, we can see that most of the typhoons bringing out peak surges over 1 m passed to the west. This fact coincides with information obtained by Okuyama and Unoki (11).

Table 1 Frequency of η_{max} and R_T (upper line: 1900-1949; lower line: 1950-1980)

	R_T<20 mm	R_T>20 mm	Total
η_{max}<26 cm	119 109	74 45	193 154
η_{max}>26 cm	15 39	20 43	35 82
Total	134 148	94 88	228 236

Table 2 Frequency of η_{max} for two groups of data: east and west of Osaka Bay (1900-1980)

η_{max} (cm)	East	West	Total
150<η_{max}	0	7	7
100<η_{max}	2	17	19
50<η_{max}	20	42	62
26<η_{max}	42	75	117

Typhoon Location When η_{max} Occurred

Several typhoon tracks causing η_{max} over 1 m at Osaka are shown in Fig. 1, which demonstrates that the high storm surges occurred when typhoons passed westward and parallel to the apse line of Osaka Bay. Especially, we can point out from all the typhoon data causing large storm surge disasters, as were reported by Okuyama and Unoki (11), that η_{max} occurred after, or immediately after, the typhoons have passed through Osaka Bay.

Figure 2 shows the spatial distribution of typhoon locations at the time when η_{max} occurred. The outlines of regions of η_{max} over 1, 1.5, and 2 m, respectively, seem to be nearly the ellipses, and the regions become smaller with increasing η_{max}. The occurrence field of η_{max} for the west-course typhoons causing large surges is clearly characterized by that the apse lines of η_{max}=1, 1.5 and 2 m are nearly perpendicular to the apse line of Osaka Bay.

Typhoon Location When r_p Occurred

The spatial distribution of typhoon locations, when the peak rainfall

intensities r_p (mm/hr) occurred, is shown in Fig. 3. Being different from the case of η_{max} mentioned above, the occurrence field of r_p cannot be divided into two groups: the east and the west regions, and it is seen that the spatial distribution of r_p is fairly random. This may be due to the fact that the rainfalls associated with typhoons are affected by many complicated factors: such as geographical features, local meteorological conditions, distributions of typhoon cumulonimbus and water vapor contents.

Relationship between η_{max} and r_p

The histogram of the time-lag τ of occurrence between η_{max} and r_p is shown in Fig. 4, where the positive sign of τ is used when r_p

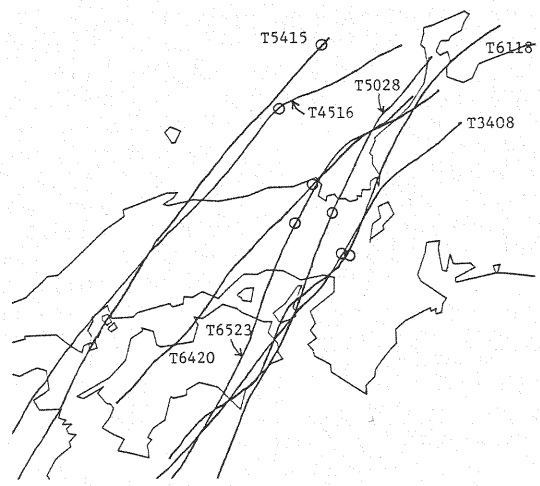

Fig. 1 Observed typhoon tracks causing η_{max} over 1 m at Osaka (symbol ○ : typhoon location when η_{max} occurred).

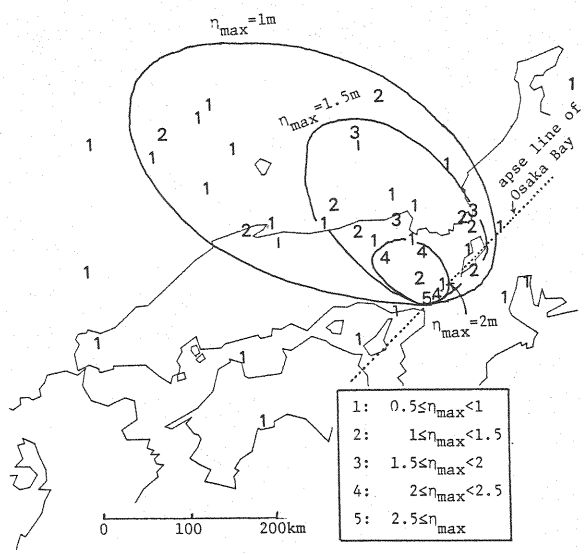

Fig. 2 Distribution of typhoon locations when η_{max} occurred.

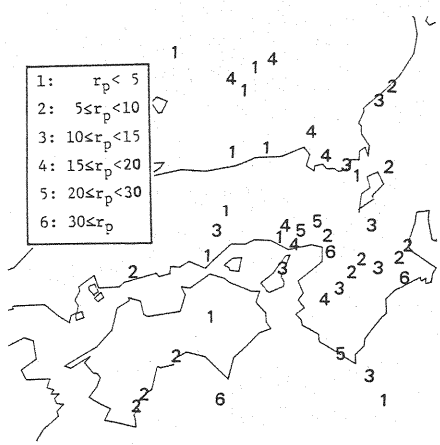

Fig. 3 Distribution of typhoon locations when r_p occurred.

precedes η_{max}. The distribution-shape of τ is nearly symmetrical as a whole. However, when the data is classified as either the east or the west of the apse line of Osaka Bay and moreover classified as either L<100 km or L>100 km where L is the vertical distance from a typhoon location (at the time when η_{max} occurred) to the apse line of Osaka Bay, the distributions of these four groups are considerably different from one another. The frequency of a range of occurrence time-lag: $-2 \leqq \tau \leqq 2$ (hrs.) between η_{max} and r_p is 41 percent and especially the time-lags of typhoons causing η_{max} over 1 m are found to be almost in this range.

Figure 5 shows the relationship between η_{max} and r_p using τ as a parameter. With increasing η_{max}, τ seems to be smaller; namely, the possibility of concurrence of η_{max} and r_p seems to be larger. It is worth notice that the upper observed limits of r_p against η_{max} are due to typhoons with the time-lag τ in the region of

-1∿1 hour, for a wide range of η_{max}.

The joint probability of two variates: x and y has been formulated based on a marked point process theory (14) and Freund's bivariate exponential distribution (2) in which the cross-correlation between x and y is taken into consideration (Hashino (3)). Application of this method to the couple of η_{max} and r_p for the past typical typhoons gives the joint return period: Txy as shown in Table 3, where the other return period: Tx·Ty that neglects the cross-correlation between η_{max} and r_p, is also shown as a reference. It can be clearly found from Table 3 that taking the cross-correlation coefficient (=-0.16) into account fairly reduces the joint return period; namely, if the correlation is neglected, the return period is over-estimated.

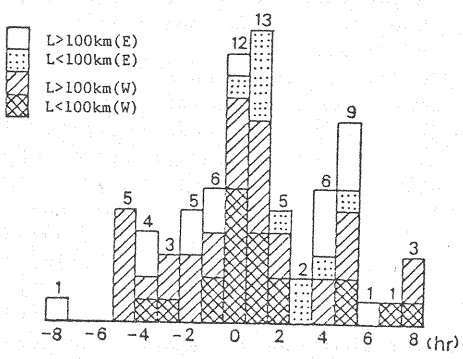

Fig. 4 Histogram of time-lag τ (positive sign is used when r_p precedes η_{max}).

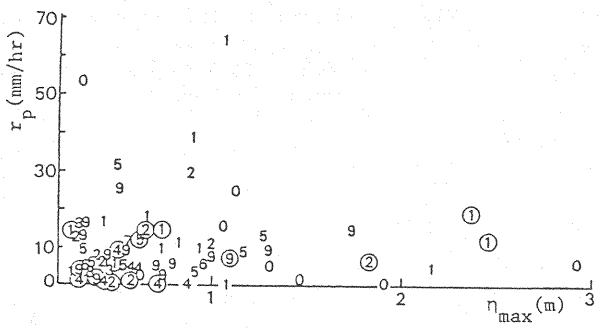

Fig. 5 Relationship between r_p and η_{max} (figure: τ(hr), symbol ○ : negative sign of τ).

Table 3 Joint return periods for the past three typhoons

Typhoon Name	Date	r_p (mm/hr)	η_{max} (cm)	T_{xy} (yr)	T_x T_y (yr)
Muroto	21/09/'34	6.8	292	215	485
Jane	03/09/'50	19.8	237	240	560
T 7916	30/09/'79	64.5	107	338	785

Relationship between η_{max} and R_T

The relationship between η_{max} and the total rainfall R_T is shown in Fig. 6, where the vertical distance L is used as a parameter. The upper observed limits of R_T seem to be smaller with increasing η_{max}. They are due to the west-course typhoons for η_{max}>1.1 m and due to the east-course ones for η_{max}<1.1 m. In each case mentioned above, the typhoons related to the upper limits of R_T are found to pass through the region within the vertical distance of L=100 km.

REGRESSION ANALYSES AGAINST RAINFALL AND STORM SURGE

By using the hourly typhoon information (typhoon location, central pressure, moving direction, moving velocity, etc.), the stepwise regression analyses against hourly rainfall intensity (mm/hr) and storm surge (cm) at Osaka are performed.

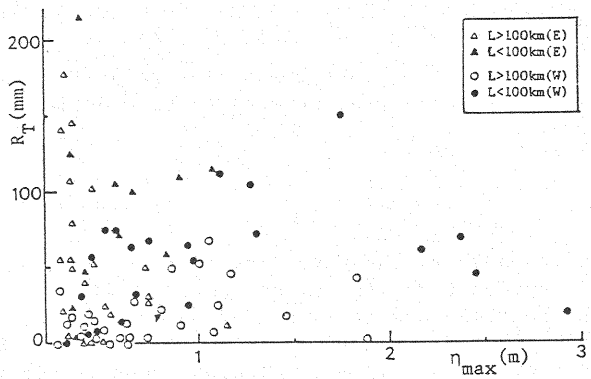

Fig. 6 Relationship between R_T and η_{max}.

The pressure P_X at a specific point X, that is employed as a variable in the regression analysis, is estimated by Schloemer's formula (13):

$$P_X = P_T + \Delta P_T \exp(-y_M/y) \tag{1}$$

where ΔP_T=1013-P_T; P_T = central pressure of a typhoon (mb); y = distance from a typhoon center to a specific point; y_M = radius from a typhoon center to the point that yields the maximum of the cyclostrophic wind velocity, assumed to be 80 km. Moreover, the vector components of the friction free wind derived from composition of a typhoon moving velocity vector and the gradient wind vector of which the direction angle is assumed to be 30° inside in the isobar direction are adopted as the wind speed V_X and wind direction θ_X at a specific point X.

Regression Analysis against Storm Surge

Since the typhoon course, the east or the west of Osaka, makes a large difference in the characteristics of the storm surge, the stepwise regression analysis is performed for each data of east- and west-course typhoons. As for the regression analysis, η_{max} (cm) is adopted as a dependent variable, while nine independent variables considered are as follows: ΔP_T(=1013 - P_T); θ_T = moving direction of a typhoon; θ_{TO} = direction of a segment y from a typhoon center to Osaka; y_M/y; y_M/L_O (where L_O is the vertical distance from a typhoon to the apse line of Osaka Bay); ΔP_O and ΔP_C = difference between the pressures at Osaka and the center of Osaka Bay calculated by Eq. 1, respectively, and the outer pressure (assumed to be 1013 mb); and $V_O^2\cos\phi_O$ and $V_C^2\cos\phi_C$ = parallel components of the squared friction free wind velocity to the direction of the apse line, at Osaka and the center of Osaka Bay, respectively. By the stepwise regression analysis, the following equations are obtained:

$$\text{East:}\quad \eta_{max} = 13.45(y_M/y) + 0.02V_C^2\cos\phi_C + 37.4 \tag{2}$$

$$\text{West:}\quad \eta_{max} = 2.02\Delta P_O - 0.04V_C^2\cos\phi_C + 0.08V_O^2\cos\phi_O + 24.4 \tag{3}$$

where the multiple correlation coefficient R and the sample size N to Eqs. 2 and 3 are R=0.65, N=41 and R=0.86, N=83, respectively. As for the east-course typhoons with η_{max} almost less than 1 m, the multiple correlation coefficient R is not high. As for the west-course typhoons including large surges, however, R is high and Eq. 3 seems to suggest that main causes of the large storm surges are the wind draft effect and the barometric effect.

Assuming that Eqs. 2 and 3 for η_{max} can be also applicable to the hourly storm surge η, the distributions of the residual: $\varepsilon = \eta - \tilde{\eta}$ in which $\tilde{\eta}$ represents the estimate by Eqs. 2 and 3, are examined. Each of the residual ε for east- and west-course typhoons follows approximately the normal distribution, and the auto-correlation coefficients of ε are high (0.808 and 0.736, respectively) for both east- and west-course typhoons.

Regression Analysis against Rainfall

It is theoretically derived by Syono (15) that the hourly rainfall intensity r in the lower stratum of symmetric cyclones is proportional to the vorticity ζ of the gradient wind velocity Vg as

$$\zeta = \frac{1}{y}\frac{\partial(yVg)}{\partial y} \tag{4}$$

Therefore, against the dependent variable r, the vorticity ζ of the gradient wind velocity is employed as one of independent variables, and besides ΔP_0, θ_{T0}, $L_0 = y \cdot \sin\phi_0$ and these variables with the time-lags of -1 and -2 hours which are represented by the subscripts of the variables are regarded as independent variables.

In the light of the distribution of the typhoon locations when r_p occurred, as is shown in Fig. 3, the data regions of concentric circles with their center at Osaka and with radiuses of D=100, 200, and 300 km, respectively, are set for the stepwise regression analysis. As a result, the following equations are selected:

$$0 \leqq D < 100 \text{ (km)}: \quad r = 0.39r_{-1} + 2.48\zeta_{-1} - 1.58\zeta_{-2} + 1.13 \tag{5}$$

$$100 \leqq D < 200 \text{ (km)}: \quad r = 1.75\zeta + 0.56r_{-1} + 0.28 \tag{6}$$

$$200 \leqq D < 300 \text{ (km)}: \quad r = 2.99\zeta + 0.38r_{-1} + 0.34 \tag{7}$$

$$D \geqq 300 \text{ (km)}: \quad r = 0.12\Delta P_0 + 0.002L_0 + 0.37 \tag{8}$$

where the multiple correlation coefficient R and the sample size N against Eqs. 5∿8 are R=0.65, N=108; R=0.63, N=255; R=0.56, N=294; and R=0.3, N=292, respectively. Consequently the ratio of the random component to the hourly rainfall intensity seems to be fairly large. For the region within the radius of D=300 km, the distribution of the relative residual: $w = (r - \check{r})/\check{r}$ where $\check{r}$ = estimated intensity by Eqs. 5∿7, r = observed intensity, is examined, and it is clarified that the transformed series W by the equation:

$$W = (w + 1)^{4/5} \tag{9}$$

follows Freund's bivariate exponential distribution.

A data generation technique composed of the regression models obtained herein for the rainfall and the storm surge associated with a typhoon and the stochastic typhoon model (Hashino and Kuwata (4)) can provide useful information to evaluate the characteristics of concurrence of the rainfall and the storm surge associated with a typhoon.

RIVER WATER LEVEL IN CASE OF CONCURRENCE OF FLOOD FLOW AND STORM SURGE

Concurrence of Flood Flow and Storm Surge in the River

As described above, typhoons are frequently accompanied by both the rainfalls in the river basin and the storm surges with a short time-lag. Accordingly, it is quite within the range of possibility that a flood wave travels down a river and a storm surge runs up the river, simultaneously. If the flood flow and storm surge concur in the river course, they interact with each other and water levels in the tidal reach will become considerably higher than those caused by the flood flow or by the storm surge independently.

The characteristics of propagation of flood waves in a river for the fixed lower boundary condition, namely the constant water level at the river mouth, were described in various literature, for example, the book by Mahmood and Yevjevich (10), and the studies on storm surges running up a river in case of the constant discharge as the upper boundary condition were also reported by Ichiye (7) and Hayami et al.(5). Nevertheless, the literature treating the behavior of water

movement in a river for concurrence of flood flow and storm surge has been scarcely found (Konishi and Kinoshita (9)). In the subsequent articles, we make the quantitative evaluation of its concurrent effect and reveals the mechanism of interaction between a flood flow and a storm surge through close analyses of the running-up behavior of storm surges.

Governing Equation and Numerical Method of Solution

We make the one-dimensional analysis for flood waves travelling down and storm surges running up a river, by neglecting the influence of density difference between river water and sea water. Then, the governing equations for flood flow and storm surge are given by

$$\frac{\partial Q}{\partial t} + \frac{\partial}{\partial x}\left(\frac{Q^2}{A}\right) + gA\left(\frac{\partial h}{\partial x} + S_f - S_0\right) = 0 \tag{10}$$

$$\frac{\partial A}{\partial t} + \frac{\partial Q}{\partial x} = 0 \tag{11}$$

where Q = discharge; A = cross-sectional area of flow; h = water depth; S_0 = river-bed slope; S_f = friction slope, $S_f = (n^2 Q|Q|)/(R_a^{4/3} A^2)$; R_a = hydraulic radius; and n = Manning's roughness coefficient.

Numerical simulations are carried out by using the Preissmann four-point implicit scheme (12), which transforms Eqs. 10 and 11 into the following form (Kanda et al. (8), Cunge et al. (1)):

$$Q_{i+1}^{n+1} + Q_i^{n+1} - Q_{i+1}^n - Q_i^n + 2\theta\frac{\Delta t}{\Delta x}\left\{\left(\frac{Q^2}{A}\right)_{i+1}^{n+1} - \left(\frac{Q^2}{A}\right)_i^{n+1}\right\} + 2(1-\theta)\frac{\Delta t}{\Delta x}\left\{\left(\frac{Q^2}{A}\right)_{i+1}^{n} - \left(\frac{Q^2}{A}\right)_i^{n}\right\}$$

$$+ g\Delta t\{\theta(A_{i+1}^{n+1} + A_i^{n+1}) + (1-\theta)(A_{i+1}^n + A_i^n)\}\left[\frac{\theta}{\Delta x}(h_{i+1}^{n+1} - h_i^{n+1}) + \frac{(1-\theta)}{\Delta x}(h_{i+1}^n - h_i^n)\right.$$

$$\left. + \frac{1}{2}\{\theta(S_{f,i+1}^{n+1} + S_{f,i}^{n+1}) + (1-\theta)(S_{f,i+1}^n + S_{f,i}^n)\} - S_0\right] = 0 \tag{12}$$

$$A_{i+1}^{n+1} + A_i^{n+1} - A_{i+1}^n - A_i^n + 2\theta\frac{\Delta t}{\Delta x}(Q_{i+1}^{n+1} - Q_i^{n+1}) + 2(1-\theta)\frac{\Delta t}{\Delta x}(Q_{i+1}^n - Q_i^n) = 0 \tag{13}$$

where Δt = time between two computational intervals; Δx = distance between two computational points in x-direction; n = time step index; i = computational point index; and θ = weighting coefficient.

Boundary Conditions

The river channel used for numerical simulations is 30 km long and has a rectangular cross-section and a bed slope of 1/3000, as shown in Fig. 7. Numerical analyses are made for three kinds of boundary conditions. Firstly, as the boundary condition for flood flows are given the time-varying discharge q_f at the upper boundary and a constant water level at the river mouth. Secondly, as the boundary condition for storm surges are given a constant discharge at the upper boundary and the time-varying water level H_d at the river mouth. We give the variations of q_f and H_d with respect to time as follows:

$$q_f = \begin{cases} a_f \sin\{(t-c_f)\pi/b_f\} + a_f + q_0 & (t_f^i \leq t \leq t_f^e) \\ q_0 & (t < t_f^i,\ t > t_f^e) \end{cases} \tag{14}$$

$$H_d = \begin{cases} a_s \sin\{(t-c_s)\pi/b_s\} + a_s + H_0 & (t_s^i \leq t \leq t_s^e) \\ H_0 & (t < t_s^i,\ t > t_s^e) \end{cases} \tag{15}$$

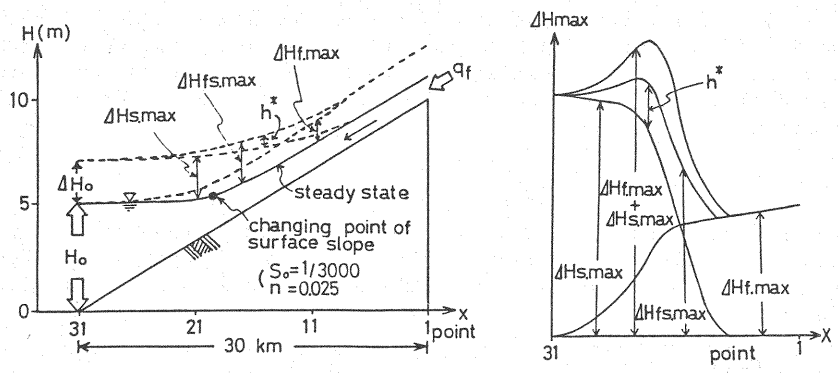

Fig. 7 Highest water level along river channel.

where q_f = discharge per unit width of channel; q_0 and H_0 = constant discharge and water level in the steady state; t^1 and t^e = time when q_f or H_d begins to increase and time when it becomes to the steady state again, respectively; and a, b and c = constants.

Thirdly, for concurrence of flood flow and storm surge, the boundary condition is set as follows. The flood discharge and the water level at both boundaries vary with time as expressed by Eqs. 14 and 15, and they have the time-lag between their peaks, as shown in Fig. 8. The positive sign of time-lag; $\tau>0$ indicates that the peak of flood discharge at the upper boundary occurs ahead of the peak of storm surge at the river mouth, and the storm surge occurs ahead of the flood discharge for $\tau<0$.

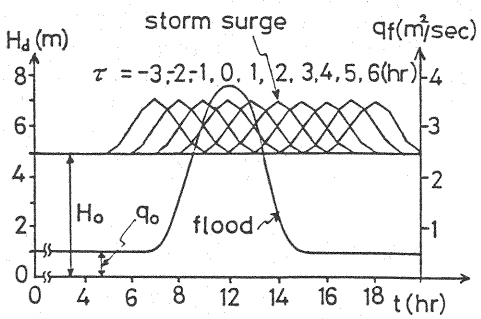

Fig. 8 Flood discharge at the upper boundary and water level at the river mouth due to storm surge.

Result of Computation

An example of water surface profiles for concurrence of a flood flow and a storm surge is shown in Fig. 9, where τ=2 hours. The highest water levels at

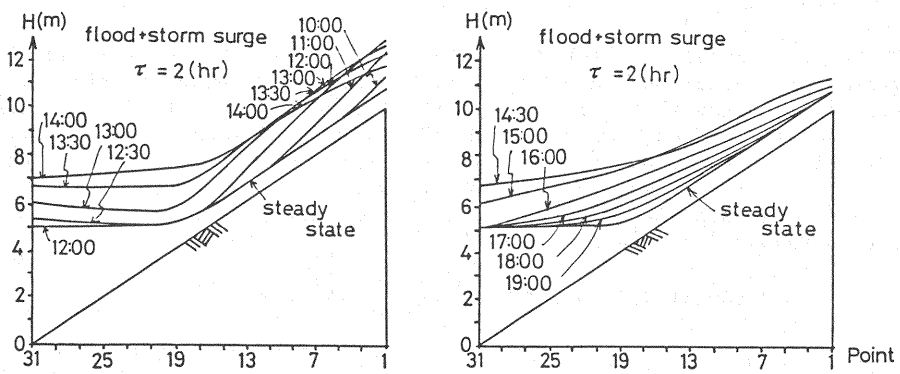

Fig. 9 Water surface profiles for τ=2 hours.

points along the river are schematically shown for the above mentioned three kinds of boundary conditions in Fig. 7, where ΔHmax represents the maximum increase in water depth measured from the water surface in the steady state before a flood flow and/or a storm surge occur. Increases ΔHf.max and ΔHs.max refer to the flood flow for the first boundary condition and the storm surge for the second boundary condition mentioned above, respectively. The former attenuates abruptly downstream from the changing point of water surface slope in the steady state, and the latter does so upstream from that point. Increase ΔHfs.max refers to the maximum increase in water depth due to concurrence of flood flow and storm surge.

The concurrent effect is denoted by h^*, that is,

$$h^* = \Delta Hfs.max - \max(\Delta Hf.max, \Delta Hs.max) \tag{16}$$

The magnitude of h^* depends not only on the distance from the downstream end, but also on the time-lag τ, and it approaches zero as τ approaches the positive or negative infinity. Figure 10 shows the magnitude of h^* along the river channel for several values of τ. Arrow marks denote the points at which the highest water

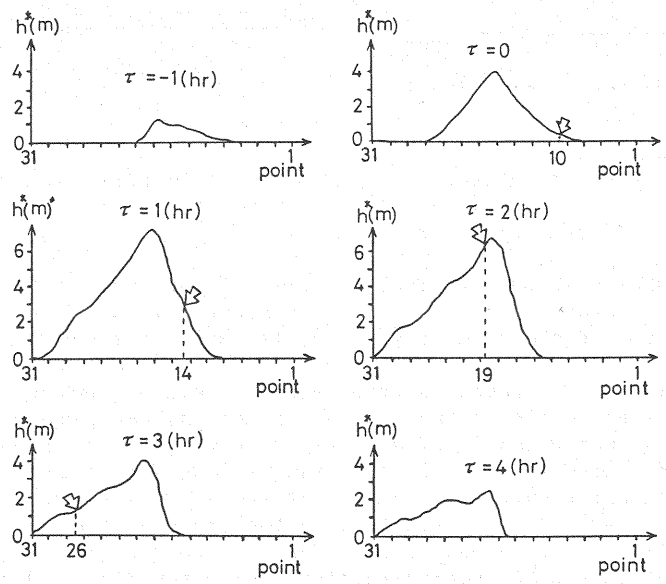

Fig. 10 Depth h^* along river channel for different length of time-lag.

level of flood flow and that of storm surge would meet if each of them separately travels downstream and upstream, respectively. For all values of τ, h^* is largest at Point 17 to Point 19 near the changing point of water surface slope. And for such time-lag that both the highest water levels of flood flow and storm surge meet at this point, namely τ=1∿2 hours, the magnitude of h^* becomes remarkably large over the whole tidal reach.

These characteristics of the highest water levels should certainly result from the interaction between flood flow and storm surge. The authors try to explain such characteristics through the following treatment. On the assumption that the flood flows are quasi-steady, the discharge at the upper boundary is kept constant while the storm surge runs up a river. Then, its running-up behavior is examined for various magnitude of the flood discharge and the duration-time of storm surge, and the relationships between the highest water level and those quantities are investigated.

CHARACTERISTICS OF STORM SURGES RUNNING UP THE RIVER

Boundary Conditions

Figure 11 shows the river channel for simulations which is the same channel as used above, except that the length of a tidal reach in the steady state is longer.

At the upper boundary (Point 1), the discharge q_f is kept constant, and at the river mouth (Point 51) are given the variations of water level with time due to the storm surges as shown in Fig. 12.

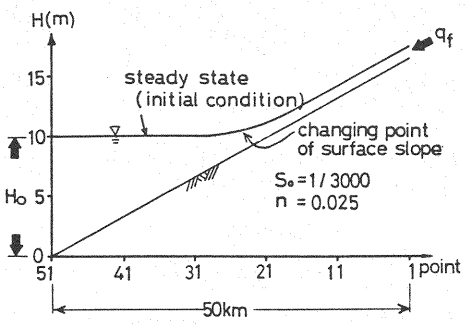

Fig. 11 Water surface profile in the steady state.

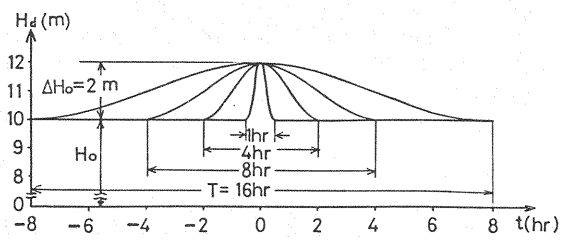

Fig. 12 Water level due to storm surge at river mouth.

Wave Motion in Running-up of Storm Surge

Figure 13 shows the longitudinal profiles of increased water depth for several duration-time T of storm surges, where ΔH is measured from the water surface in the steady state. For the short duration-time, T=1 hour, the surface profile changes in the manner of the wave with a single crest, and the velocity of propagation as well as the wave height abruptly decreases near the upper end of the tidal reach. For T=8 hours, water levels at the upstream points are already raised to rather higher elevations than water level at a river mouth when it reaches the peak (t=0). For the longer duration-time, T=16 hours, water levels move up and down with the almost horizontal water surfaces. Figure 14 shows the water surface profiles near the highest water levels. Dot-dash-line is the trace of the wave crest $A(x_0,y_0)$, and the broken line the envelope of the highest water level $B(x_1,y_1)$. If the wave height attenuates in the upstream direction as is seen for T=1 hour, the highest water level propagates before the wave crest. If it increases as is seen for T=4 hours, the wave crest propagates before the highest water level. In this way, the running-up behavior of storm surge whose wave length is far long compared with the length of a tidal reach seems to be essentially different from the ordinary wave motion. In this connection, it is examined whether storm surges travel in the nature of the long wave, in a following manner.

Figure 15 shows the relationships between ΔH and the flow velocity v at the river mouth by broken lines, where v_0 is the velocity of the steady flow before a storm surge occurs. On the other hand, the particle-velocity of the long wave with a finite amplitude in the channel of constant water depth is expressed by the following formula, which is indicated by a solid line in the figure:

$$v_L = 2\sqrt{gH_0}\left\{\sqrt{1 + \frac{\Delta H}{H_0}} - 1\right\} \qquad (17)$$

where H_0 = water depth; and ΔH = surface elevation measured from undisturbed water surface. Although Eq. 17 is an approximation to the ΔH-v_L relationship in case of the long wave and river flow coexisting in a channel, this figure shows that water movement caused by storm surges is obviously different from that of the ordinary

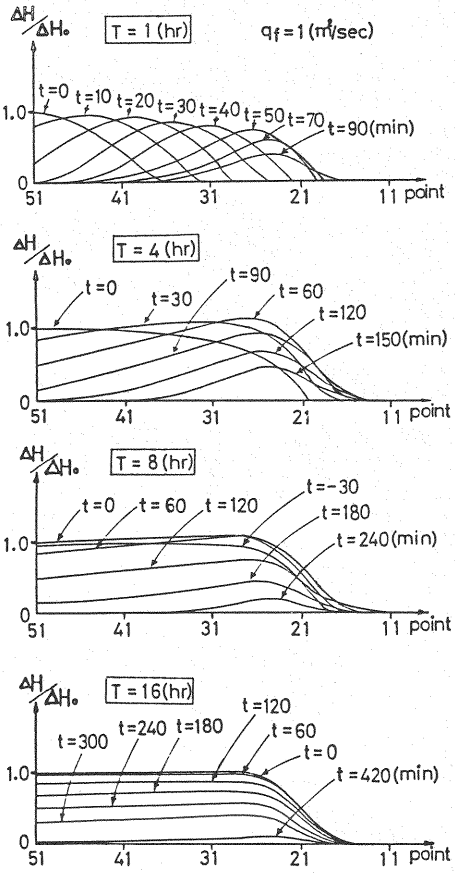

Fig. 13 Running-up behavior of storm surges for different duration-time.

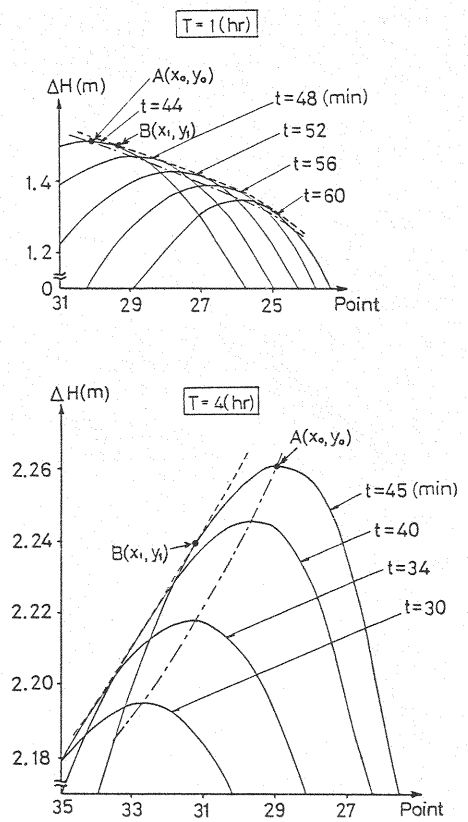

Fig. 14 Propagation of highest water level and wave crest.

long wave except the portion near the wave front. In the other words, wave theory will not be directly applicable to propagation of the highest water levels of storm surges in the tidal reach.

Figure 16 shows the time-distance relations which trace the propagation of highest water level, wave crest and maximum discharge of the reverse current caused by invasion of the storm surge, respectively. The maximum discharge propagates before the highest water level, which is the similar property to that of the flood wave travelling down a river (Henderson (6)).

Highest Water Level along River Channel

Figures 17 and 18 show the highest water levels or the maximum increases in water depth ΔHmax for several duration-time of storm surges and for several discharges at the upper boundary, respectively. The broken lines in Fig. 17 represent the heights of wave crests which are seen in Fig. 13 for T=1 and T=4 hours.

In Fig. 17, ΔHmax for T=16 hours corresponds

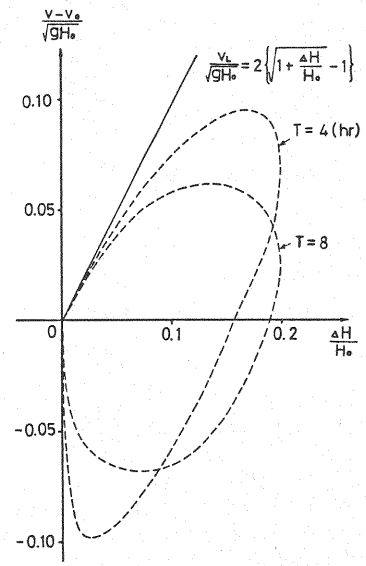

Fig. 15 Relation between water level and velocity.

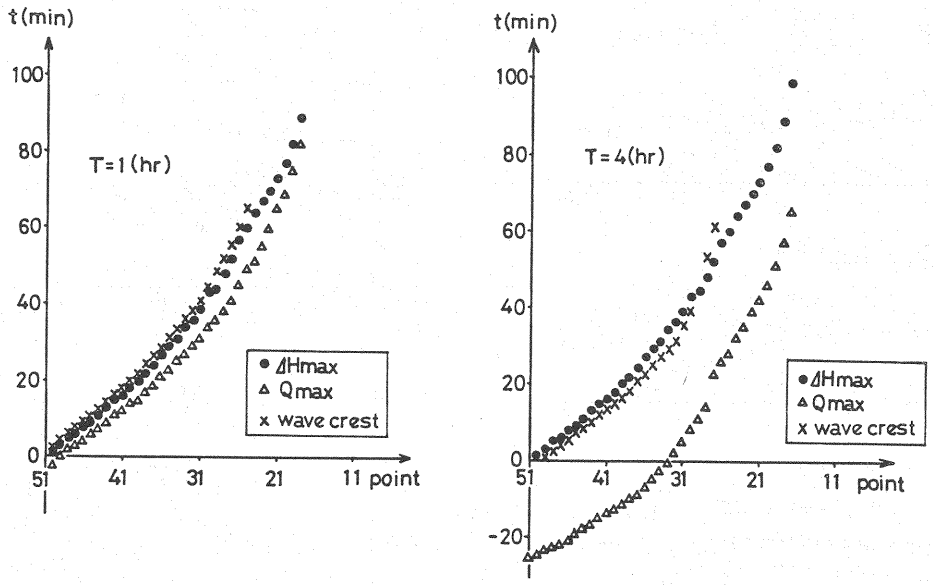

Fig. 16 Propagation of wave crest, highest water level and maximum discharge.

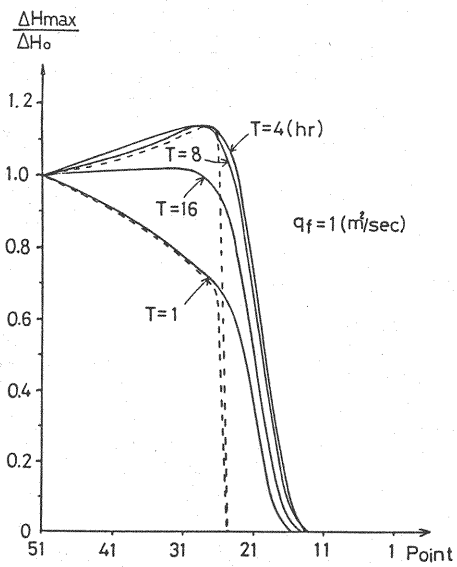

Fig. 17 Increase ΔHmax for different duration-time of storm surge.

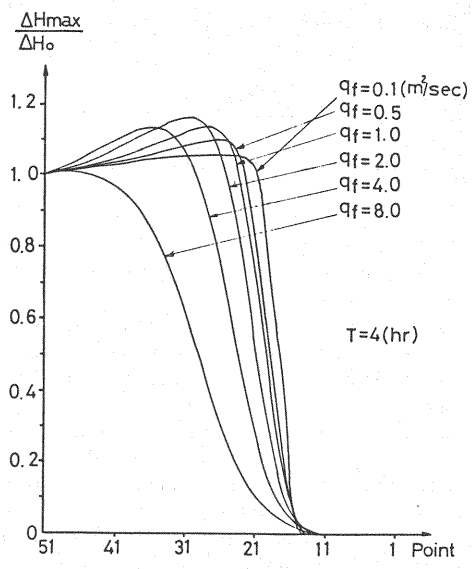

Fig. 18 Increase ΔHmax for different river discharges.

nearly with the surface profile of the steady flow when water level at the river mouth is kept constant at the peak water-elevation of storm surge, while the result for T=1 hour suggests that the highest water level attenuates more sharply as the duration-time T becomes enough short. For the intermediate duration-time, T=4 and 8 hours, water levels are rather higher over the whole tidal reach. This result substantiates that there exists a duration-time for which river water level rises to the maximum height. Similarly, Fig. 18 demonstrates the existence of a river discharge for which water level becomes highest, because water levels for q_f=1∿4 $m^2 s^{-1}$ are higher than those for the larger and the smaller discharges.

Process of Rising of Water Level in Tidal Reach

Figure 19 shows the variations of water depth h and discharge q with time at several points along the river. In case of the positive discharge the river water flows downstream, while in case of the negative discharge the reverse current due to invasion of storm surge flows upstream. The shadowed portion represents the water volume of storm surge stored at the upstream side of each point. Let this water volume be denoted by q*:

$$q^* = \int_{t_1}^{t_2} \{q_f - q(x,t)\}dt \qquad (18)$$

where q_f = constant discharge; $q(x,t)$ = discharge which is a function of x and t; and t_1 and t_2 = time when reverse current begins and ends, respectively.

The relations of q* with duration-time of storm surge and with river discharge are shown in Figs. 20 and 21, respectively. It is apparent that there exists such duration-time and river discharge for which q* becomes largest, respectively. These relations are in agreement with the above mentioned relationships between ΔHmax and duration-time of storm surge, river discharge.

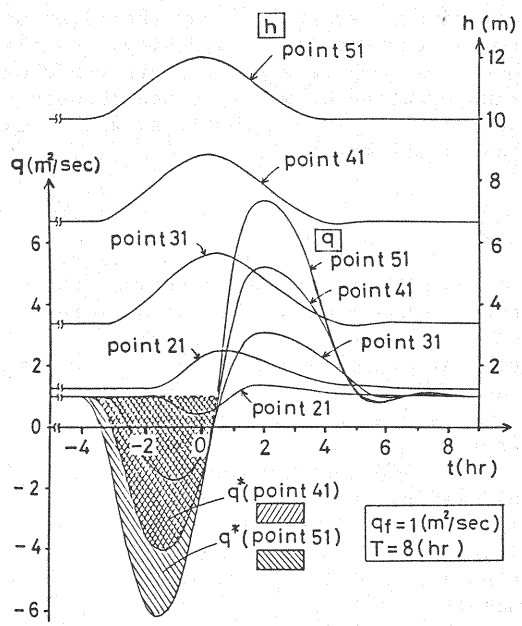

Fig. 19 Variations of water depth and discharge with time.

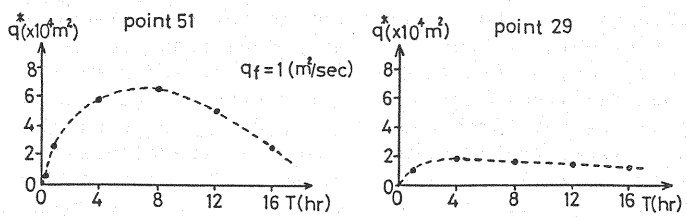

Fig. 20 Relationship between q* and duration-time of storm surge.

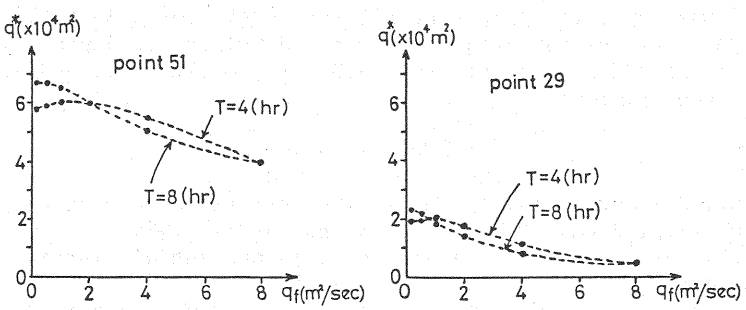

Fig. 21 Relationship between q* and river discharge.

In the light of this correspondence between ΔHmax and q*, the process of rising of water levels in the tidal reach could be explained as follows. Water level at a river mouth is raised due to a storm surge, which is accompanied by intrusion of sea water from the river mouth and also followed by production of the reverse current in its vicinity. As the intruded water increases in volume, the zone of strong reverse currents would extend to the upstream direction. This transportation of water volume through the reverse current increases water depth even at the upstream sections, and it leads to rising of water levels over the whole tidal reach.

CONCLUSIONS

The results obtained in this study are summarized as follows:

1. The relationship between the maximum storm surge η_{max} and the rainfall in Osaka has been investigated by the available data of typhoons. The frequency of the range of occurrence time-lag: $-2 \leqq \tau \leqq 2$ (hrs.) between η_{max} and the peak rainfall intensity r_p is about 40 percent, and the time-lags for almost all of typhoons causing η_{max} over 1 m are in this range. The upper observed limits of r_p against η_{max} are due to typhoons with the time-lag in the region of $-1 \sim 1$ hour for a wide range of η_{max}.

2. The spatial distribution of η_{max} depends mainly on the typhoon course; the east or the west of Osaka, while that of r_p is fairly random. The stepwise regression analyses have been carried out against two groups of η_{max} which are divided into the east and west of Osaka, and against four groups of hourly rainfall intensity r which are divided into regions of concentric circles with a center at Osaka.

3. On the occasion that the flood flow and the storm surge concur in a river, the highest water levels depend significantly on the length of time-lag between them. And for a certain time-lag, its concurrent effect becomes remarkably large almost over the tidal reach.

4. As for the running-up behavior of storm surges for the constant river discharges, water surface profiles for the long duration-time vary with time in a considerably different manner from that of the ordinary wave motion as seen in deformation of the long wave. The dominant factor of rising of river water levels is the transportation of water volume through the reverse current. Total volume of the intruded sea water, which induces the reverse current, becomes largest for a certain river discharge and a certain duration-time of storm surge. Thus, river water levels also become highest for a certain discharge and a certain duration-time. Water levels along the river under the condition of such discharge and duration-time have to yield the previously described characteristics, that is, the concurrent effect is remarkably large for the specified time-lag between flood flow and storm surge, because the flood flows are quasi-steady and their discharges are regarded as nearly constant for some duration time.

ACKNOWLEDGEMENTS

This work was supported partly by a Grant-in-Aid for Scientific Research (57020040) of Ministry of Education, Science and Culture of Japan. The authors wish to express their gratitude to Prof. A.Murota, Osaka Univ. and Prof. H.Kikkawa, Waseda Univ. for helpful advice.

REFERENCES

1. Cunge, J.A., F.M. Holly and A. Verwey : Practical Aspects of Computational River Hydraulics, Pitman Publ. Limited, pp.53-131, 1980.
2. Freund, J.E. : A bivariate extension of the exponential distribution, Jour. the American Statistical Association, Vol.56, pp.971-977, 1961.
3. Hashino, M. : On the joint probability of two hydrologic variates following a marked point process, Proc. 28th Japanese Conference on Hydraulics, pp.391-396, 1984 (in Japanese).

4. Hashino, M. and Y. Kuwata : Simulation of storm surge and rainfall using a stochastic typhoon model, Proc. 29th Japanese Conference on Hydraulics, pp.278-292, 1985 (in Japanese).
5. Hayami, S., K. Yano, S. Adachi and H. Kunishi : Experimental studies on meteorological tsunamis travelling up the rivers and canals in Osaka City, Disaster Prevention Research Institute, Kyoto Univ., Bull. No.9, pp.1-47, 1955.
6. Henderson, F.M. : Open Channel Flow, Macmillan Publ. Co., Inc., 1966.
7. Ichiye, T. : On the abnormal high waters in rivers, The Oceanographical Magazine, Vol.5, No.1, pp.45-60, 1953.
8. Kanda, T. and T. Kitada : An implicit method for unsteady flows with lateral inflows in urban rivers, Proc. 17th Congress of IAHR, Vol.2, pp.213-220, 1977.
9. Konishi, T. and T. Kinoshita : Studies on the river invasion of the storm surge (II), The Rep. of the National Research Center for Disaster Prevention, No.34, pp.13-42, 1985 (in Japanese).
10. Mahmood, K. and V. Yevjevich, ed. : Unsteady Flow in Open Channels, Water Resources Publ., 1975.
11. Okuyama, K. and S. Unoki : General description of storm tides on the coasts of Japan, Jour. Meteorological Research, JMA, Vol.11, No.6, pp.57-68, 1959 (in Japanese).
12. Preissmann, A. : Propagation des intumescences dans les canaux et rivières, First Congress of French Association for Computation, Grenoble, 1961.
13. Schloemer, R.W. : Analysis and synthesis of hurricane wind patterns over Lake Okeechobee, Florida, Hydrometeorological Report, No.31, pp.1-49, 1954.
14. Snyder, D.L. : Random Point Processes, John Wiley & Sons, Inc., New York, 1975.
15. Syono, S. : Approximate solution of non-linear differential equations of stationary wind in the lower stratum of symmetric cyclones and anticyclones and their applications, Geophys. Mag., Vol.20, pp.39-65, 1940.

APPENDIX - NOTATION

The following symbols are used in this paper:

A = cross-sectional area of flow;

D = radius of circle with a center at Osaka;

h = river water depth;

h^* = water depth representing the concurrent effect of flood flow and storm surge;

H = water level at arbitrary point along river channel;

H_d = water level at river mouth;

H_0 = water level at river mouth in the steady state;

ΔH = increase in water depth due to flood flow and/or storm surge, measured from water surface in the steady state;

$\Delta Hmax$ = maximum increase in water depth at arbitrary point along river channel;

ΔH_0 = maximum increase in water depth at river mouth;

i = computational point index (subscript);

L = vertical distance from typhoon location at the time when the maximum storm surge occurred to apse line of Osaka Bay;

L_0 = vertical distance from typhoon center to apse line of Osaka Bay;

n = Manning's roughness coefficient; time step index (superscript);

N = sample size;

P_T = central pressure of typhoon;

P_X = atmospheric pressure at a given point;

ΔP_T, ΔP_O, ΔP_C = differences between the central pressure of typhoon, the pressures at Osaka and the center of Osaka Bay calculated by Eq. 1, and the outer pressure assumed to be 1013 mb;

Q = river discharge;

q = river discharge per unit width of channel at arbitrary point along river channel;

q^* = water volume of storm surge stored at the upstream side of each point along river channel;

q_f = discharge per unit width of channel at the upper boundary;

q_0 = constant discharge per unit width of channel in the steady state;

R = multiple correlation coefficient;

Ra = hydraulic radius;

R_T = total rainfall;

r, $\check{r}$ = observed and estimated values of hourly rainfall intensity;

r_p = peak rainfall intensity;

S_0 = river-bed slope;

S_f = friction slope;

T = duration-time of storm surge;

Tx, Ty = return periods of variates: x and y;

Txy = joint return period of two variates: x and y;

Δt = time between two computational intervals;

v = flow velocity;

v_L = particle-velocity of long wave with finite amplitude;

v_0 = flow velocity in the steady state;

Vg = gradient wind velocity;

V_O, V_C = friction free wind velocities at Osaka and the center of Osaka Bay;

V_X = friction free wind velocity at a given point;

w = relative residual of hourly rainfall;

W = series transformed from w by Eq. 9;

Δx = distance between two computational points in x-direction;

y = distance from a typhoon center to a given point;

y_M = radius from a typhoon center to the point that yields the maximum of cyclostrophic wind velocity, assumed to be 80 km;

ε = residual of hourly storm surge;

ζ = vorticity of gradient wind;

η, $\check{\eta}$ = observed and estimated values of hourly storm surge, respectively;

η_{max} = maximum value of storm surge due to typhoon;

θ = weighting coefficient of Preissmann's implicit scheme;

θ_T = moving direction of typhoon;

θ_{TO} = direction of a segment y from a typhoon center to Osaka;

θ_X = friction free wind direction at a given point;

τ = time-lag between r_p and η_{max}; time-lag between the peaks of flood wave and storm surge; and

ϕ_O, ϕ_C = angles between apse line of Osaka Bay and segments from a typhoon center to Osaka and to the center of Osaka Bay, respectively.